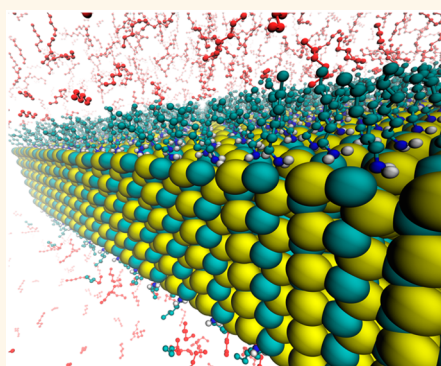# Reverse Non-Equilibrium Molecular Dynamics Demonstrate That Surface Passivation Controls Thermal Transport at Semiconductor−Solvent Interfaces

Daniel C. Hannah,[†] J. Daniel Gezelter,[‡] Richard D. Schaller,[†,§] and George C. Schatz*,[†]

[†]Department of Chemistry, Northwestern University, Evanston, Illinois 60208, United States, [‡]Department of Chemistry and Biochemistry, University of Notre Dame, Notre Dame, Indiana 46556, United States, and [§]Center for Nanoscale Materials, Argonne National Laboratory, Argonne, Illinois 60439, United States

ABSTRACT We examine the role played by surface structure and passivation in thermal transport at semiconductor/organic interfaces. Such interfaces dominate thermal transport in semiconductor nanomaterials owing to material dimensions much smaller than the bulk phonon mean free path. Utilizing reverse nonequilibrium molecular dynamics simulations, we calculate the interfacial thermal conductance (G) between a hexane solvent and chemically passivated wurtzite CdSe surfaces. In particular, we examine the dependence of G on the CdSe slab thickness, the particular exposed crystal facet, and the extent of surface passivation. Our results indicate a nonmonotonic dependence of G on ligand-grafting density, with interfaces generally exhibiting higher thermal conductance for increasing surface coverage up to ∼0.08 ligands/$Å^2$ (75−100% of a monolayer, depending on the particular exposed facet) and decreasing for still higher coverages. By analyzing orientational ordering and solvent penetration into the ligand layer, we show that a balance of competing effects is responsible for this nonmonotonic dependence. Although the various unpassivated CdSe surfaces exhibit similar G values, the crystal structure of an exposed facet nevertheless plays an important role in determining the interfacial thermal conductance of passivated surfaces, as the density of binding sites on a surface determines the ligand-grafting densities that may ultimately be achieved. We demonstrate that surface passivation can increase G relative to a bare surface by roughly 1 order of magnitude and that, for a given extent of passivation, thermal conductance can vary by up to a factor of ∼2 between different surfaces, suggesting that appropriately tailored nanostructures may direct heat flow in an anisotropic fashion for interface-limited thermal transport.

KEYWORDS: nanocrystals · thermal transport · nonequilibrium molecular dynamics · phonons · heat conduction · simulations

Thermal management critically affects the performance of virtually all semiconductor devices. For example, light-emitting and light-harvesting technologies benefit from maximal thermal conductivity in the photoactive layer, while thermoelectric materials benefit from low thermal conductivity. Therefore, strategies for manipulating the thermal conductivity can directly improve device functionality. Semiconductor nanocrystals (SNCs), which exhibit size-tunable energy gaps and are amenable to low-cost solution-phase processing, have been proposed as a means to improve the performance of all the device types mentioned above. However, SNCs necessarily present greatly elevated surface-to-volume ratios and interfaces on a

nanometer length scale. It was recently demonstrated that the interfacial thermal conductance between the SNCs and the material surrounding them (often, but not always a hydrophobic, long-chain hydrocarbon) plays a critical role in mediating the thermal conductivity of the overall composite.[1] However, this interface is difficult to access experimentally; at present, the only estimates of interfacial thermal conductance for a SNC and its surroundings rely on fits to a modified effective medium theory[1] or lower-bound estimates based on characterization of thermal transport rates *via* optical spectroscopy.[2] Such measurements yield only averaged information regarding the thermal transport, and the quality of available data is typically such

that fits to effective medium theories yield estimates with 100% or greater uncertainties.[1] Theoretical modeling can provide microscopic insight into the underlying physics and guide the rational design of nanoscale materials with tailored thermal properties. While theoretical models such as the diffuse mismatch model and the acoustic mismatch model are commonly applied in the calculation of interfacial thermal conductance,[3,4] these models do not work well above cryogenic temperatures[5] and it is not readily apparent how such models could be applied to a chemically passivated interface.[6] Atomistic methods such as molecular dynamics simulations are therefore an appealing method for extracting the interfacial thermal conductance of heterogeneous systems at ambient temperatures.

Numerous studies have applied molecular dynamics simulations to the calculation of interfacial thermal conductance in nanoscale systems containing a solid, a chemical passivating layer, and/or a matrix material. However, much of this work focuses on systems where the solid is metallic, such as self-assembled alkanethiol monolayers on gold surfaces,[6−8] gold nanoparticles,[9,10] or nanocrystal arrays containing ligand-passivated gold building blocks.[1,11] To date, no theoretical study and few experimental studies have examined the interfacial thermal conductance of semiconductor−organic systems common to the colloidal preparations described above, such as metal chalcogenides. Here, we apply reverse nonequilibrium molecular dynamics (RNEMD) simulations to the calculation of interfacial thermal conductance in hexane-solvated, hexylamine-passivated CdSe interfaces, an extremely common experimental configuration for colloidal SNCs. First, we demonstrate that a simple potential originally parametrized by Rabani[12] to reproduce structural transformations and phonon dispersion relations is also capable of accurately describing thermal conductivity in CdSe. With a suitable potential for the modeling of thermal processes, we then examine interfacial thermal conductance for interfaces presenting the four wurtzite surfaces common to CdSe nanostructures: the $11\overline{2}0$ and $10\overline{1}0$ surfaces, which are nonpolar, and the 0001 and $000\overline{1}$ surfaces, which are polar. The role played by surface passivation is examined and estimates of interfacial thermal conductance are obtained for realistic CdSe interfaces. Furthermore, we examine the important role played by surface atomic density in establishing upper limits on the interfacial thermal conductance.

THEORY

A variety of theories exist for the calculation of interfacial thermal conductance (henceforth denoted G) from molecular dynamics simulations. Time-correlation functions, such as the heat flux autocorrelation function (HFACF), can be computed from the results of equilibrium molecular dynamics (EMD) simulations. These time-correlation functions can be used to compute various transport coefficients for the system being simulated, including the interfacial thermal conductance. However, EMD-based methods typically exhibit slow convergence of the HFACF for systems containing grain boundaries and low interfacial thermal conductance,[13] as might be expected of a system containing acoustically mismatched components. Nonequilibrium molecular dynamics (NEMD) methods can be preferable in such cases as less simulation time is required to achieve the steady-state temperature gradient necessary to compute G. Traditionally, NEMD methods impose a gradient on a simulation cell and measure the resulting flux, which can then be used to compute transport properties. However, as it is not apparent what type of gradient should be enforced at interfaces, RNEMD methods are better suited to the study of such systems. In RNEMD simulations of thermal conductivity, an unphysical heat flux is imposed between different regions of the simulation cell. The system responds by developing a temperature gradient between those regions. The resulting temperature gradient can be then be used to compute thermal conductivity as well as G. RNEMD approaches have been applied successfully to metal/organic systems in the past[6−8,10] and will be used here for the study of semiconductor (CdSe)/organic systems. The RNEMD simulations in this work utilize a velocity shearing and scaling (VSS) algorithm, the details of which are reported elsewhere[14] but will be described briefly below and in the Supporting Information for this work.

The original momentum swapping procedure developed by Müller-Plathe[15,16] generally works well for describing the thermal conductivity of bulk liquids, but exchange moves perturb the system away from thermal distributions and at large momentum flux values, the resulting "notched" temperature gradients fall outside of the linear response regime required in order to utilize Fourier's law in the derivation of G.[17] To address these issues, we utilize a recently developed VSS technique which applies velocity shearing and scaling exchanges between the two slabs.[14] Such exchanges are subject to a set of constraints which ensure that new configurations are sampled from an NVE ensemble. In comparison to the original Müller-Plathe method, VSS-RNEMD distributes flux more evenly within the exchange regions and avoids strong perturbations. The enforcement of thermal sampling and wide distribution of imposed flux reduces the development of nonlinear temperature gradients. Furthermore, the VSS-RNEMD method can create a flux between atoms of arbitrary identity without efficiency losses due to differences in particle mass, making VSS-RNEMD an ideal method for heterogeneous systems.[14] The mathematical details of the VSS-RNEMD algorithm can be found in the Supporting Information.

As described above, an unphysical heat flux, J_z, is imposed between "hot" and "cold" regions in the simulation cell, with the exchange axis denoted Z. Eventually, a steady-state temperature gradient develops between the two regions. Using the slope of this temperature gradient, it is simple to obtain the thermal conductivity of the simulation cell, denoted λ, using eq 1:

$$J_z = -\lambda \left(\frac{\partial T}{\partial z} \right) \quad (1)$$

For systems containing one or more interfaces, the regions on either side of an interface will develop relatively homogeneous, but distinct, temperatures. The temperature difference at these interfaces can be used to derive the interfacial thermal conductance, G, as shown in eq 2:

$$G = \frac{J_z}{\Delta T} \quad (2)$$

While other definitions, formulated in terms of temperature derivatives, exist for the interfacial thermal conductance, the form shown in eq 2 was shown to be both straightforward in its application and in good agreement with experimental values for a gold–alkanethiol interface.[6] It is this form which we will utilize in the work detailed below. In systems containing multiple interfaces, this method can be applied by calculating the total thermal boundary resistance (R_K, the inverse of G) for a series of thermal resistors:

$$G^{-1} = R_K = \sum_{i=1}^{n} R_i = \sum_{i=1}^{n} \frac{T_{i+1} - T_i}{J_z} = \frac{T_n - T_1}{J_z} \quad (3)$$

It is necessary to demonstrate the suitability of any interaction potential used in a classical molecular dynamics simulation for simulating the physical properties or processes of interest. In his original work, Rabani fitted Coulombic and Lennard-Jones potential energy parameters to reproduce the elastic constants and phonon dispersion relations of CdSe.[12] The form of the interaction potential is shown in eq 4:

$$V_{ij} = \left(\frac{q_i q_j}{r_{ij}} \right) + 4\epsilon_{ij} \left[\left(\frac{\sigma_{ij}}{r_{ij}} \right)^{12} - \left(\frac{\sigma_{ij}}{r_{ij}} \right)^{6} \right] \quad (4)$$

In eq 4, q_i is the charge on atom i, r_{ij} is the distance between atoms i and j, ϵ_{ij} is the depth of the potential energy well, and σ_{ij} is the distance at which the interparticle potential is zero. The Rabani interaction potential has been shown to reproduce well the Hamaker constant of bulk CdSe as well as the pressure-induced phase transition from the ambient-pressure wurtzite to the high-pressure rocksalt phase.[12] The Rabani potential has also been shown to accurately capture the transition of CdSe nanostructures from a wurtzite to rocksalt phase at pressures elevated relative to the bulk transition.[18,19] Furthermore, the Rabani potential has been shown to accurately reproduce the

size-dependent phonon frequencies and electron–phonon coupling (based on an effective-mass wave function model) in CdSe nanoparticles.[20] Here, we demonstrate the applicability of the Rabani potential to the calculation of thermal conductivity in bulk CdSe. Figure 1a shows the temperature gradient developed during a RNEMD simulation of a 30 Å × 30 Å × 400 Å slab of wurtzite CdSe. A target flux of 695 MW/m² was imposed, with kinetic energy exchanges occurring every 5 fs. Figure 1b displays the inverse of thermal conductivity values displayed for a range of system lengths having an identical cross-section. As the finite size of the simulation cell artificially truncates the phonon mean free path compared to a true bulk system, it is necessary to account for finite size effects.[21] A linear fit of this data, shown as a dotted line in Figure 1b, may be used to extrapolate to the true bulk thermal conductivity, as shown by eq 5:

$$\frac{1}{\lambda(\infty)} = \frac{1}{\lambda(L)} + \frac{C}{L} \quad (5)$$

In eq 5, λ is the thermal conductivity, C is a constant, and L is the length of the simulation cell along the kinetic energy flux direction. Extrapolation to infinite length yields a thermal conductivity of 6 ± 2 W/m/K, which is firmly within the range of experimental thermal conductivity values (4–9 W/m/K) reported for bulk, crystalline CdSe at 300 K.[22−24] Computational methods and simulation protocol are detailed in the Methods section of the manuscript.

RESULTS AND DISCUSSION

Having established that the Rabani interaction potential is well-suited for the simulation of thermal conductivity in bulk wurtzite CdSe, we now simulate the interfacial thermal conductance of various CdSe surfaces passivated and solvated by organic ligands. Figure 2a details the chemically distinct components used to model solvent molecules in the simulations presented here (see the Methods section for further details). The temperature profile resulting from a 3 ns RNEMD simulation of a CdSe(11$\bar{2}$0)/hexane interface is shown in Figure 2b. Utilizing eq 8, we obtain an interfacial thermal conductance of ~8 MW/m²/K for a 40 Å long slab. As with simulations of infinite, bulk materials, RNEMD simulations show convergence in the interfacial thermal conductance with respect to the size of the system. The dependence of G on slab thickness arises from the disordering of atoms near the interface, resulting in an altered vibrational power spectrum with respect to the bulk atoms. In thin slabs, all atoms are close to an interface and therefore exhibit similar vibrational power spectra. This similarity yields higher G values for thinner slabs. To isolate finite size effects from interfacial conductance, we performed RNEMD simulations on a series of slab lengths. The length of
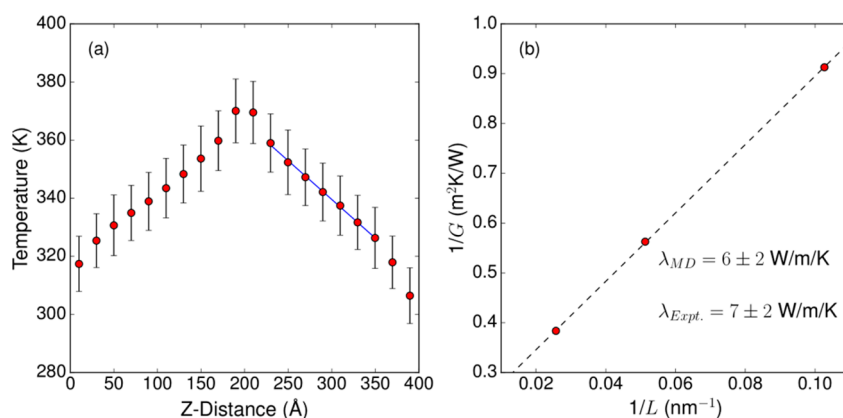
Figure 1. (a) Temperature profile along the kinetic energy exchange axis obtained following a 3 ns RNEMD simulation of a wurtzite CdSe slab. The solid blue line indicates a linear fit to the linear response region of the temperature profile. The slope of this line is used to obtain thermal conductivity *via* eq 1. (b) Inverse thermal conductivity (obtained as described above) as a function of inverse length. Extrapolation to the *y*-intercept yields the bulk (*i.e.*, infinite length) thermal conductivity. Simulated (λ_{MD}) and experimental (λ_{expt}) values of thermal conductivity for CdSe are given on the figure. Uncertainty values for λ_{MD} were obtained from the average of four statistically independent RNEMD simulations, while the standard deviation in λ_{expt} is obtained from an average of reported literature values.[22−24]
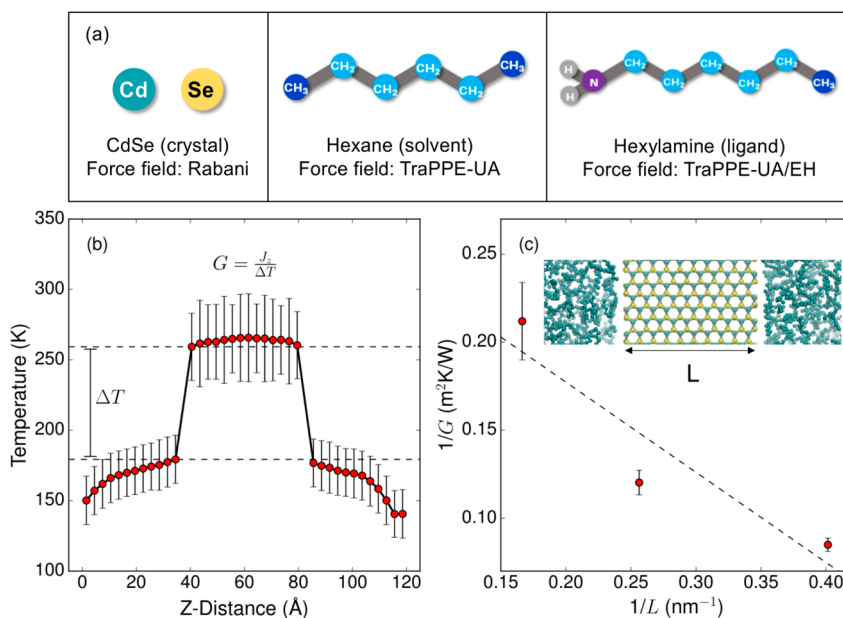

Figure 2. (a) Topologies of the molecules used in our simulations. The chemically distinct sites, given as colored spheres in the above diagram, are treated as united atoms. Amine headgroups are modeled with explicit hydrogen atoms. Parameters are obtained from ref 23. (b) Temperature profile along the kinetic energy exchange axis obtained for a system containing hexane and an unpassivated CdSe 11$\bar{2}$0 slab. The discontinuities near 40 and 80 Å represent the CdSe/hexane interface. The temperature drop at this interface, indicated by a dashed line in 3a, is used to obtain the interfacial thermal conductance, *G*. (c) Inverse interfacial thermal conductance as a function of inverse slab length, *L*. As the length of the solvent region is also increased for larger simulations (fixed at 2*L*), extrapolation to the *y*-intercept yields the interfacial thermal conductance for an infinitely thick slab of CdSe surrounded by an infinitely thick hexane bath. Inset: A snapshot from an MD trajectory used to produce this data. *L* is indicated on the figure.

the hexane portion of the simulation cell was increased proportionally in each simulation. A fitting procedure similar to eq 5 may be used obtain *G* values for a CdSe/hexane interface propagating to infinite length in the kinetic energy flux direction on either side of the interface. Figure 2c displays the *G* value obtained for 3 CdSe(11$\bar{2}$0) slabs of increasing thickness. The inset of Figure 2c displays a snapshot of the CdSe(11$\bar{2}$0)/hexane interface, taken from one of the trajectories used to

produce the data. Similar simulations were performed for the 10$\bar{1}$0, 000$\bar{1}$, and 0001 surfaces. These surfaces are of particular interest as they are the exposed surfaces of most CdSe nanocrystals.[25] Each of the surfaces yields a similar value for the interfacial thermal conductance (2−3.5 MW/m^2/K). The results of our calculations for a bare CdSe/hexane interface are summarized in Table 1.

Next, we probe the effects of surface passivation on the interfacial thermal conductance of the

CdSe/hexane interface. Figure 3 displays the temperature profile obtained for a completely passivated hexylamine-passivated $11\bar{2}0$ surface. Here, complete passivation is defined as having one hexylamine ligand for each surface atom, as described in the Methods section. The temperature profile obtained here is more complicated owing to compositional heterogeneity and multiple interfaces. In this case, eq 3 is applied in the calculation of the interfacial thermal conductance. The interfacial thermal conductance values obtained for fully passivated hexylamine-passivated CdSe surfaces are summarized in Table 2. To obtain average values of G, we performed four statistically independent RNEMD simulations of each surface. Statistical independence was ensured by generating initial velocity distributions

from a different random seed for each replicated simulation.

As shown in Table 2, the presence of a passivating layer significantly increases the interfacial thermal conductance of a CdSe/hexane interface. This elevated thermal conductance can be understood in terms of improved vibrational overlap between CdSe and hexylamine as well as between hexane and hexylamine. Figure 4a displays the vibrational power spectrum of each distinct molecular component in the simulation cell (CdSe, hexylamine, hexane). The vibrational power spectrum is obtained by taking the Fourier transform of a velocity autocorrelation function obtained from 3 ns of simulation in an NVE ensemble subsequent to the pre-equilibration steps described above. This is shown in eq 6:

$$f(\omega) = \int_{-\infty}^{+\infty} \langle \vec{v}_A(t) \cdot \vec{v}_A(0) \rangle e^{-2\pi i t \omega} dt \qquad (6)$$

The hexylamine layer, shown in the middle of Figure 4a, clearly exhibits greatly improved vibrational overlap with hexane, as these molecules are structurally and compositionally similar. Hexylamine also exhibits greater overall vibrational overlap with CdSe than hexane. This is emphasized in Figure 4b, which

TABLE 1. RNEMD-Derived Interfacial Thermal Conductance Values for Four Surfaces of Wurtzite CdSe

surface	G^a (MW/m^2/K)
$11\bar{2}0$	3.6 ± 0.9
$10\bar{1}0$	1.7 ± 0.5
0001	2.0 ± 0.6
$000\bar{1}$	1.9 ± 0.6

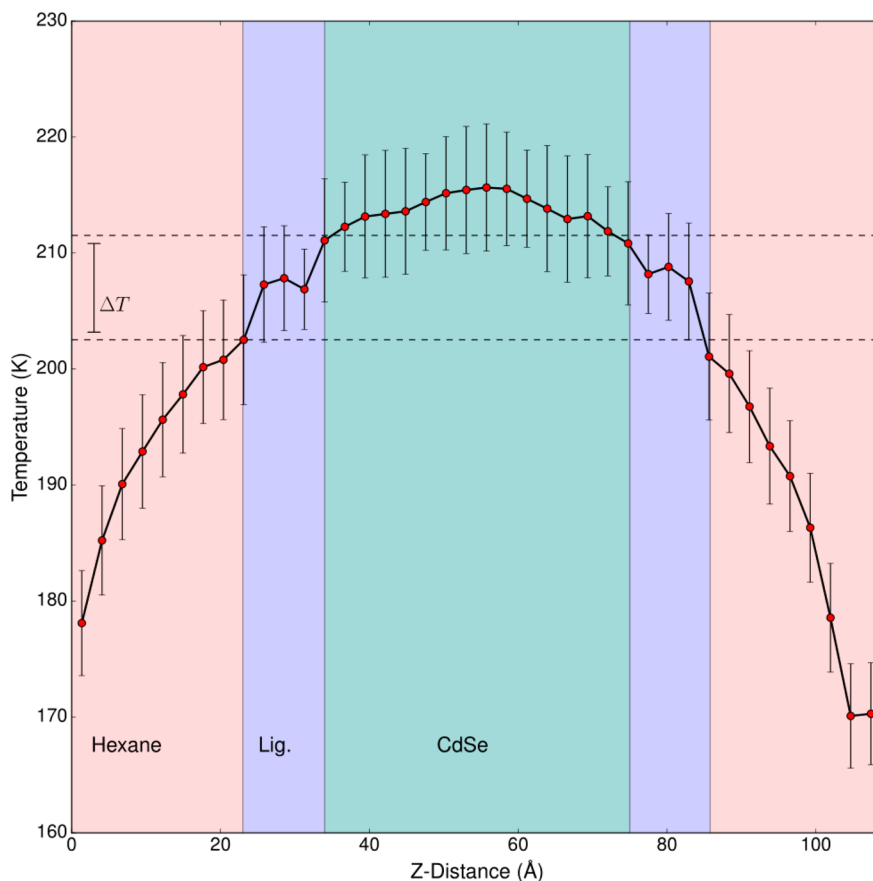^{a} Error estimates are derived from linear fits to the size dependence of G.

Figure 3. Temperature profile along the kinetic energy exchange axis obtained following a 3 ns RNEMD simulation of a system containing hexane (solvent) and a CdSe($11\bar{2}0$) slab passivated by hexylamine (ligand). The Z-coordinates corresponding to each region are labeled on the figure, with interfaces being designated by dashed lines.

focuses on the low frequency region containing the CdSe vibrational modes.

We also explore the dependence of interfacial thermal conductance on the extent of surface passivation. Figure 5a displays the interfacial thermal conductance as a function of ligand density on the surface, with each G value (and its uncertainty) being the average (and

standard deviation) of values obtained from four statistically independent RNEMD runs, as described above. Here, ligand density is defined as the number of hexylamine molecules in the simulation cell divided by the cross-sectional area of the CdSe slab. For the nonpolar $11\bar{2}0$ and $10\bar{1}0$ surfaces, G increases roughly linearly with the extent of surface passivation. In contrast, the polar surfaces (0001 and $000\bar{1}$) show a nonmonotonic dependence of G on the extent of surface passivation. Note, however, that the nonpolar $11\bar{2}0$ and $10\bar{1}0$ surfaces have a much lower atomic density and therefore do not support grafting densities as large as those supported by the polar surfaces. As indicated in Figure 5a, the highest ligand densities studied represent 100% passivation of the surface, meaning that each surface site (as defined in the Methods) is interacting with a single passivating ligand. The polar CdSe surfaces have twice as many surface sites for a given cross-sectional area; this is demonstrated

TABLE 2. RNEMD-Derived Interfacial Thermal Conductance Values for Four Surfaces of Fully Passivated Wurtzite CdSe

surface	G^a (MW/m^2/K)
$11\bar{2}0$	72 ± 12
$10\bar{1}0$	80 ± 8
0001	90 ± 7
$000\bar{1}$	82 ± 11

^{a} Standard deviations are computed from the average of four statistically independent replicated simulations for each surface.
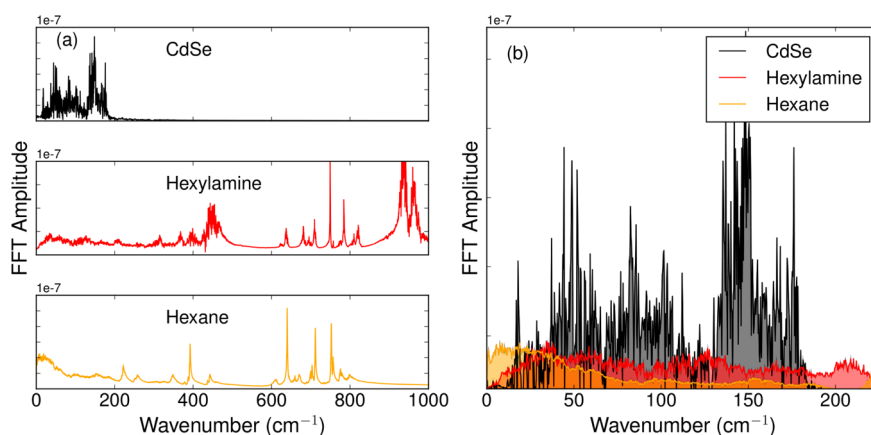

Figure 4. (a) Vibrational density of states at 200 K as obtained from Fourier transformation of the velocity autocorrelation function (eq 6) from an NVE simulation of a hexylamine-passivated, CdSe($11\bar{2}0$) surface surrounded by hexane. Each panel is labeled by molecular species. (b) Comparison of vibrational overlap at low frequencies. Hexylamine, shown in red, has a higher vibrational density of states than hexane (yellow) for most of this spectral region.
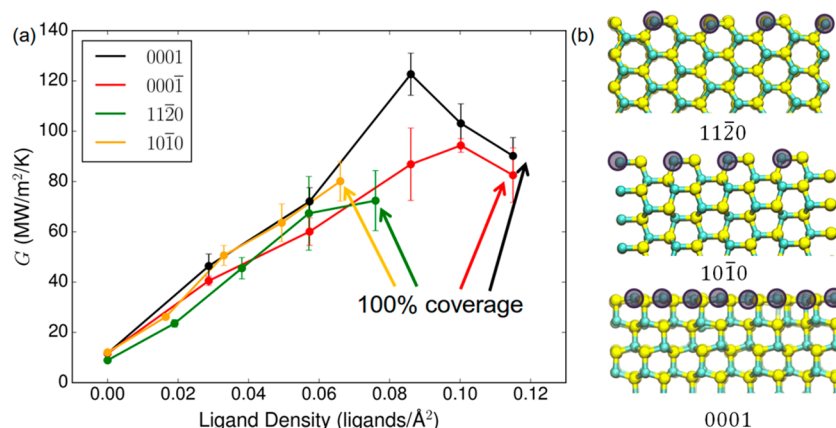

Figure 5. (a) Interfacial thermal conductance, G, as a function of ligand density on various CdSe surfaces. In this case, ligand density is defined as the number of passivating ligand molecules in the simulation cell divided by the cross-sectional area of the cell. 100% coverage, labeled on the figure, indicates the ligand density at which a given CdSe surface has a single ligand molecule interacting with each available surface Cd atom. Uncertainties are derived from statistically independent replicate runs as described in the manuscript. (b) Schematic of the nonpolar ($11\bar{2}0,10\bar{1}0$) and polar (0001) surfaces. Surface binding sites are indicated by translucent purple circles.
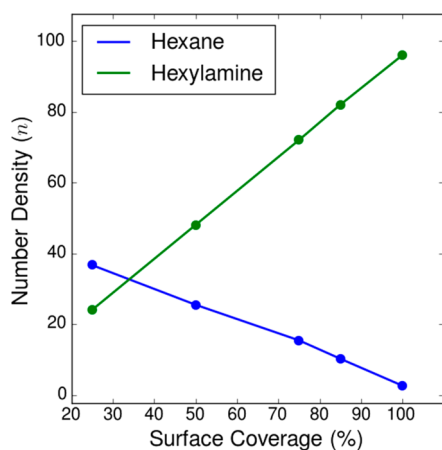
Figure 6. Integrated number density in the ligand region for ligand (hexylamine) and solvent (hexane) molecules as a function of surface coverage on a 0001/000$\bar{1}$ CdSe slab. These curves intersect at roughly 35% surface coverage.

visually in Figure 5b, which highlights the number of surface sites for the 11$\bar{2}$0, 10$\bar{1}$0, and 0001 surfaces. While no experimental estimate yet exists for the thermal conductance of CdSe/hexylamine/hexane interfaces, the G values obtained here for maximal surface coverage are qualitatively similar to values experimentally measured for an oleate-passivated PbS nanocrystal array[1] and so are likely physically reasonable.

The nonmonotonic dependence of G on surface ligand density (Figure 5A) can be understood as a balance of competing effects related to conduction, ordering, and excluded volume. First, surface ligands clearly facilitate heat conduction in the system *via* improved vibrational overlap (Figure 4). However, larger surface ligand densities also exclude solvent penetration into the ligand layer. Figure 6 displays the time-averaged number density of both hexane (solvent) and hexylamine (ligand) along the kinetic energy exchange axis as obtained from analysis of RNEMD trajectories subsequent to the development of a stable temperature gradient. Higher ligand coverages clearly coincide with reduced solvent penetration into the same region; density profiles for each coverage can be found in the Supporting Information. Ligand and solvent molecules have a roughly equal number density at ∼35% ligand coverage, which should maximize conduction effects, as every hexane molecule in the ligand layer, at least in principle, has a hexylamine partner available for coupling. This first-order analysis, however, ignores effects due to orientational ordering and solvent trapping in the ligand layer.

While low ligand coverage permits greater solvent penetration into the ligand layer, these solvent molecules are less likely to be ordered in a fashion conducive to thermal energy transfer. As molecular alignment plays an important role in facilitating thermal energy transfer,[26] the relative orientation of ligand molecules and solvent molecules in the ligand layer

must be considered. Qualitatively, it is expected that higher ligand densities will force interpenetrating solvent molecules into alignment. This effect can be examined *via* diagonalization of an order parameter tensor given by eq 7:

$$Q_{\alpha\beta} = \frac{1}{2N} \sum_{i=1}^{N} (3\mathbf{e}_{i\alpha}\mathbf{e}_{i\beta} - \delta_{\alpha\beta}) \qquad (7)$$

In eq 7, $\mathbf{e}_{i\alpha}$ is the $\alpha = x, y, z$ component of the unit vector $\mathbf{e}_i$, defined here as a vector along the terminal atoms of a given solvent or ligand molecule. The summation runs over all of the molecules being considered, with N representing the total number of molecules of a particular type (solvent or ligand). The Kroenecker delta function is represented by $\delta_{\alpha\beta}$. The largest eigenvalue of Q is traditionally used to obtain the orientational order parameter, while the eigenvector associated with that eigenvalue is the director axis, $\mathbf{d}(t)$. The director axis defines the average direction of molecular alignment at time t. The alignment of ligand molecules and entrapped solvent molecules can be quantified as the time-averaged dot product of the director axes of each respective molecule, as shown in eq 8:

$$\langle d \rangle = \langle \mathbf{d}_{\text{hexylamine}}(t) \cdot \mathbf{d}_{\text{hexane}}(t) \rangle \qquad (8)$$

This quantity ranges between 0 (hexane and hexylamine molecules aligned perpendicularly) and 1 (parallel alignment). This dot product is displayed as a function of ligand surface coverage in Figure 7a for a CdSe 0001/000$\bar{1}$ surface. Generally <d> is larger for higher surface coverages, reflecting the formation of "pockets" which force interpenetrating solvent molecules into alignment.[27] The anomalously low value of <d> for 100% surface coverage reflects the near-complete exclusion of solvent from the ligand layer (Figure 6e). This alignment facilitates efficient thermal coupling, offsetting the decreased penetration of solvent into the ligand layer.

In addition to the average density of solvent molecules in the ligand layer, the time scales of solvent movement into and out of the ligand layer are also of interest. To analyze these time scales, we utilize a survival correlation function which measures the residence time of a solvent molecule in the ligand layer. This function, $C(t)$, correlates the identity of all hexane molecules within the ligand layer at two times. If the solvent molecule is present at both times, the configuration contributes a 1, and contributes a 0 otherwise. A 0 contribution indicates that the solvent molecule has migrated back into the bulk liquid, and so a steep decay of $C(t)$ indicates a high turnover rate of solvent molecules in the ligand region. We define this solvent escape rate, k, for a simulation of duration T, according to eq 9:

$$k = \left(\int_0^T C(t)\,\mathrm{d}t \right)^{-1} \qquad (9)$$
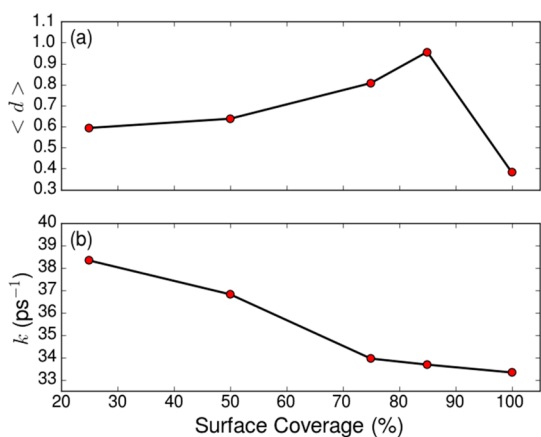
Figure 7. (a) Time-averaged dot product of the director axis for hexylamine molecules and hexane molecules present in the hexylamine layer, as defined in eq 8, as a function of surface coverage for the $0001/000\bar{1}$ surfaces. (b) Solvent escape rate, k, as a function of surface coverage for the $0001/000\bar{1}$ CdSe surfaces.

Figure 7b displays k as a function of surface coverage. As surface ligand density increases, k decreases, indicating that solvent molecules spend a longer time trapped in the ligand layer at high coverages. Depending on the time scale of heat transfer between the hexylamine ligands and hexane molecules in the ligand layer, the increased residence time of the solvent molecules at higher coverages my facilitate thermal transport by allowing the solvent molecules adequate time to thermalize with the ligands before returning to the bulk liquid. While G does decrease for surface coverages yielding the lowest k values, it is unlikely that the residence time of solvent molecules in the ligand layer is long enough to impede interfacial thermal conductance. Given the extremely small relative change in k ($\sim$2%) over the 75–100% surface coverage range, the decrease in G is more likely a result of solvent exclusion (Figure 6), which eventually overwhelms positive contributions to interfacial thermal conductance due to orientational ordering and vibrational overlap. It is the interplay of these effects which ultimately yields the nonmonotonic dependence of G on surface coverage for the polar CdSe surfaces (Figure 5a).

CONCLUSIONS

Our results highlight the important role played by surface chemistry and crystal structure in mediating thermal transport across chemically passivated semiconductor interfaces. Generally, passivation of a CdSe surface with hexylamine increases the thermal conductance of the interface by more than 1 order of magnitude. Furthermore, we find that while G increases with increasing surface coverage at lower ligand-grafting densities, G *decreases* at the highest grafting densities.

The nonmonotonic dependence of G on surface coverage is a manifestation of several competing phenomena. Hexylamine (the passivating ligand) exhibits improved vibrational overlap with both CdSe and hexane (the solvent). The presence of hexylamine thus facilitates efficient thermal coupling in the system. However, as ligand grafting on the surface becomes increasingly dense, exclusion of solvent molecules from the ligand layer occurs. At the same time, higher ligand coverage tends to force into alignment any solvent molecules which do manage to penetrate into the ligand layer, yielding more efficient vibrational coupling of these molecules. Higher coverages also result in decreased solvent escape rates, though these decreases are unlikely to play a dominant role in determining G. Taken in aggregate, these effects produce maximal interfacial thermal conductance at ligand-grafting density values in the range of 0.08–0.1 ligands/Å^2. These grafting density values represent a fractional coverage that varies for a particular facet. For the nonpolar surfaces ($10\bar{1}0$, and $11\bar{2}0$), a ligand-grafting density of 0.08 represents a full monolayer (all binding sites occupied), while the same grafting density represents roughly 75% of a monolayer for the polar surfaces (0001 and $000\bar{1}$). The ligand-grafting density corresponding to a full monolayer (100% coverage) for each surface is indicated in Figure 5a.

While the interfacial thermal conductance of bare CdSe surfaces was found to be similar for each of the surfaces studied, crystal structure nevertheless plays an extremely important role, as the number of available binding sites on each surface ultimately determines the limit of ligand-grafting density. For example, for the wurtzite crystal structure, passivated nonpolar surfaces exhibit much lower interfacial thermal conductance than passivated polar surfaces owing to fewer binding sites per unit area of the nonpolar surface. As synthetic methods for semiconductor nanocrystals have become increasingly sophisticated, particularly for metal chalcogenide nanocrystals, chemical control of the surface areas of each facet has become a possibility. Our results therefore have interesting implications for the synthetic manipulation of interfacial thermal conductance in this technologically important material class.

The specific case of a crystalline CdSe semiconductor material was examined this work, but the phenomena identified are general. The dependence of ligand-grafting density (and, thus, interfacial thermal conductance) on the particular exposed surface is a previously unreported phenomenon; prior studies examining gold surfaces find that ligand-grafting density is primarily determined by the steric behavior of the ligands. This effect likely stems from the fact that CdSe is a binary compound and only half of the exposed atoms on a nonpolar surface will interact strongly with ligands, resulting in lower overall grafting density for these surfaces. The hexagonal lattice and different structural parameters of CdSe as

compared to Au may also play a role. Regardless, our results highlight for the first time the possibility of atomic structure on the exposed crystal surface being the primary factor in determining the interfacial thermal conductance of chemically passivated interfaces. In the limit that interfacial thermal conductivity dictates the overall thermal transport rate involving a semiconductor, variation in the surface termination and exposed surface area offers a route to anisotropic transport that can aid thermoelectric efficiencies or improve heat dissipation from LEDs, lasers, and solar cells.

METHODS

Our simulations utilize a combination of united-atom (UA) and explicit hydrogen (EH) parameters for the TraPPE force field.[28] The TraPPE model includes parametrizations for bonding interactions including stretches, bends, dihedrals, and torsions. For the amine terminal of the hexylamine molecules, TraPPE-EH parameters were used to model N and explicit H atoms to account for any role played by H in determining the packing of ligand monolayers on the CdSe surface. All other hydrocarbons utilized the TraPPE-UA model. Previous simulations of thermal conductivity which compared a similarly parametrized all-atom force field (OPLS-AA) to the TraPPE-UA did not find a significant difference in the thermal conductivity obtained from RNEMD simulations between the two force fields. Thus, the TraPPE-UA models are computationally efficient while maintaining accuracy.[6]

To construct CdSe surface/solvent interface models, a slab of crystalline (wurtzite) CdSe having a fixed cross-section of 30 Å × 30 Å was built having a particular crystalline direction oriented along the z-axis of the simulation cell and then equilibrated at 200 K and 1 atm. For the systems studied here, 125 ps of equilibration time was found to be sufficient to ensure stable thermodynamic variables. Following equilibration in the NPT and NVT ensembles, the simulation cell was expanded along the z-axis to twice the length of the wurtzite slab. This empty space was filled with hexane molecules to experimental density at 200 K using the PackMOL algorithm.[29] The simulation cell was then equilibrated again at 200 K and 1 atm first in the NPT and then NVT ensemble. After all equilibration steps were complete, RNEMD simulations were run in the NVE ensemble using a target flux of 695 MW/m^2 and an exchange time of 5 fs. RNEMD simulations were run for sufficiently long times to ensure the development of a stable temperature profile, typically 3 ns.

Passivated CdSe surfaces were constructed in a similar fashion. Hexylamine, a common experimental passivating ligand, was chosen for this study. Passivated CdSe surfaces were constructed by placing a hexylamine molecule, initially aligned along the z-axis of the simulation cell, atop each grafting site on the surface. For the $11\bar{2}0$, $10\bar{1}0$, and 0001 surfaces, hexylamine was initially placed atop Cd atoms, while for the $000\bar{1}$ surface, which is Se terminated, hexylamine was placed atop Se atoms. These placements are in agreement with density functional theory studies, which indicate that amine surface ligands primarily interact with surface Cd atoms.[30,31] After ligand placement, the system was equilibrated in an NVT ensemble to permit internal relaxation followed by equilibration at 200 K and 1 atm in the NPT ensemble. After these equilibration steps, the simulation cell was expanded to twice the length of the wurzite + ligand system and filled with hexane as before. The system was then equilibrated again at 200 K and 1 atm in the NPT and then NVT ensembles. Following these equilibration steps, RNEMD simulations were executed as described above. Ligand motion is unconstrained throughout the simulation; ligand molecules are free to sample the CdSe surface. Ligand migration occurs on the $000\bar{1}$ surface during equilibration, with ligand headgroups shifting to the interstitial sites in between surface Se atoms, situated roughly halfway between the surface Se atom and subsurface Cd atom below it. At the same time, these subsurface Cd atoms relax toward the surface. Ligand migration is minimal for the other surfaces studied here. All of the molecular dynamics simulations in this work utilized the OpenMD software package.[32]

REFERENCES AND NOTES

1. Ong, W.-L.; Rupich, S. M.; Talapin, D. V.; McGaughey, A. J. H.; Malen, J. A. Surface Chemistry Mediates Thermal Transport in Three-Dimensional Nanocrystal Arrays. *Nat. Mater.* **2013**, *12*, 410–415.
2. Hannah, D. C.; Dunn, N. J.; Ithurria, S.; Talapin, D. V.; Chen, L. X.; Pelton, M.; Schatz, G. C.; Schaller, R. D. Observation of Size-Dependent Thermalization in CdSe Nanocrystals Using Time-Resolved Photoluminescence Spectroscopy. *Phys. Rev. Lett.* **2011**, *107*, 177403.
3. Swartz, E.; Pohl, R. Thermal Boundary Resistance. *Rev. Mod. Phys.* **1989**, *61*, 605–668.
4. Little, W. A. The Transport of Heat between Dissimilar Solids at Low Temperatures. *Can. J. Phys.* **1959**, *37*, 334–349.
5. Landry, E.; McGaughey, A. Thermal Boundary Resistance Predictions from Molecular Dynamics Simulations and Theoretical Calculations. *Phys. Rev. B* **2009**, *80*, 165304.
6. Kuang, S.; Gezelter, J. D. Simulating Interfacial Thermal Conductance at Metal-Solvent Interfaces: The Role of Chemical Capping Agents. *J. Phys. Chem. C* **2011**, *115*, 22475–22483.
7. Luo, T.; Lloyd, J. R. Equilibrium Molecular Dynamics Study of Lattice Thermal Conductivity/Conductance of Au-Sam-Au Junctions. *J. Heat Transfer* **2009**, *132*, 032401–032401.
8. Luo, T.; Lloyd, J. R. Non-Equilibrium Molecular Dynamics Study of Thermal Energy Transport in Au–Sam–Au Junctions. *Int. J. Heat Mass Transfer* **2010**, *53*, 1–11.
9. Chen, X.; Munjiza, A.; Zhang, K.; Wen, D. Molecular Dynamics Simulation of Heat Transfer from a Gold Nanoparticle to a Water Pool. *J. Phys. Chem. C* **2013**, *118*, 1285–1293.
10. Stocker, K. M.; Gezelter, J. D. A Method for Creating Thermal and Angular Momentum Fluxes in Nonperiodic Simulations. *J. Chem. Theory Comput.* **2014**, *10*, 1878–1886.
11. Ong, W.-L.; Majumdar, S.; Malen, J. A.; McGaughey, A. J. H. Coupling of Organic and Inorganic Vibrational States and Their Thermal Transport in Nanocrystal Arrays. *J. Phys. Chem. C* **2014**, *118*, 7288–7295.

12. Rabani, E. An Interatomic Pair Potential for Cadmium Selenide. *J. Chem. Phys.* **2002**, *116*, 258–262.

13. Schelling, P.; Phillpot, S.; Keblinski, P. Comparison of Atomic-Level Simulation Methods for Computing Thermal Conductivity. *Phys. Rev. B* **2002**, *65*, 144306.

14. Kuang, S.; Gezelter, J. D. Velocity Shearing and Scaling Rnemd: A Minimally Perturbing Method for Simulating Temperature and Momentum Gradients. *Mol. Phys.* **2012**, *110*, 691–701.

15. Müller-Plathe, F. A Simple Nonequilibrium Molecular Dynamics Method for Calculating the Thermal Conductivity. *J. Chem. Phys.* **1997**, *106*, 6082–6085.

16. Müller-Plathe, F. Reversing the Perturbation in Nonequilibrium Molecular Dynamics: An Easy Way to Calculate the Shear Viscosity of Fluids. *Phys. Rev. E* **1999**, *59*, 4894–4898.

17. Tenney, C. M.; Maginn, E. J. Limitations and Recommendations for the Calculation of Shear Viscosity Using Reverse Nonequilibrium Molecular Dynamics. *J. Chem. Phys.* **2010**, *132*, 014103.

18. Grünwald, M.; Rabani, E.; Dellago, C. Mechanisms of the Wurtzite to Rocksalt Transformation in CdSe Nanocrystals. *Phys. Rev. Lett.* **2006**, *96*, 255701.

19. Grünwald, M.; Lutker, K.; Alivisatos, A. P.; Rabani, E.; Geissler, P. L. Metastability in Pressure-Induced Structural Transformations of CdSe/ZnS Core/Shell Nanocrystals. *Nano Lett.* **2012**, *13*, 1367–1372.

20. Kelley, A. M. Electron−Phonon Coupling in CdSe Nanocrystals from an Atomistic Phonon Model. *ACS Nano* **2011**, *5*, 5254–5262.

21. Chantrenne, P.; Barrat, J.-L. Finite Size Effects in Determination of Thermal Conductivities: Comparing Molecular Dynamics Results with Simple Models. *J. Heat Transfer* **2004**, *126*, 577–585.

22. Berger, L. I. *Semiconductor Materials*; Taylor & Francis: Florence, KY, 1996.

23. Slack, G. A. Thermal Conductivity of II-VI Compounds and Phonon Scattering by Fe^{2+} Impurities. *Phys. Rev. B* **1972**, *6*, 3791–3800.

24. Feser, J. P.; Chan, E. M.; Majumdar, A.; Segalman, R. A.; Urban, J. J. Ultralow Thermal Conductivity in Polycrystalline CdSe Thin Films with Controlled Grain Size. *Nano Lett.* **2013**, *13*, 2122–2127.

25. Puzder, A.; Williamson, A. J.; Zaitseva, N.; Galli, G.; Manna, L.; Alivisatos, A. P. The Effect of Organic Ligand Binding on the Growth of CdSe Nanoparticles Probed by Ab Initio Calculations. *Nano Lett.* **2004**, *4*, 2361–2365.

26. Shen, S.; Henry, A.; Tong, J.; Zheng, R.; Chen, G. Polyethylene Nanofibres with Very High Thermal Conductivities. *Nat. Nano* **2010**, *5*, 251–255.

27. Stocker, K. M.; Gezelter, J. D. Simulations of Heat Conduction at Thiolate-Capped Gold Surfaces: The Role of Chain Length and Solvent Penetration. *J. Phys. Chem. C* **2013**, *117*, 7605–7612.

28. Wick, C. D.; Stubbs, J. M.; Rai, N.; Siepmann, J. I. Transferable Potentials for Phase Equilibria. 7. Primary, Secondary, and Tertiary Amines, Nitroalkanes and Nitrobenzene, Nitriles, Amides, Pyridine, and Pyrimidine. *J. Phys. Chem. B* **2005**, *109*, 18974–18982.

29. Martínez, L.; Andrade, R.; Birgin, E. G.; Martínez, J. M. PACKMOL: A Package for Building Initial Configurations for Molecular Dynamics Simulations. *J. Comput. Chem.* **2009**, *30*, 2157–2164.

30. Rempel, J. Y.; Trout, B. L.; Bawendi, M. G.; Jensen, K. F. Density Functional Theory Study of Ligand Binding on CdSe (0001), (000$\bar{1}$), and (11$\bar{2}$0) Single Crystal Relaxed and Reconstructed Surfaces: Implications for Nanocrystalline Growth. *J. Phys. Chem. B* **2006**, *110*, 18007–18016.

31. Schapotschnikow, P.; Hommersom, B.; Vlugt, T. J. H. Adsorption and Binding of Ligands to CdSe Nanocrystals. *J. Phys. Chem. C* **2009**, *113*, 12690–12698.

32. Gezelter, J.; Kuang, S.; Marr, J.; Stocker, K.; Li, C.; Vardeman, C.; Lin, T.; Fennell, C.; Sun, X.; Daily, K. *Openmd, an Open Source Engine for Molecular Dynamics*; University of Notre Dame: Notre Dame, IN, 2010.